Journal of Power Sources 184 (2008) 370–374

Contents lists available at ScienceDirect

Journal of Power Sources

journal homepage: www.elsevier.com/locate/jpowsour

Short communication

Characterization of atmospheric plasma-sprayed $La_{0.8}Sr_{0.2}Ga_{0.8}Mg_{0.2}O_3$ electrolyte

Cheng-Xin Li*, Ying-Xin Xie, Chang-Jiu Li, Guan-Jun Yang

State key Laboratory for Mechanical Behavior of Materials, School of Materials Science and Engineering, Xi'an Jiaotong University, Xianning West Road 28#, Xi'an Shaanxi 710049, PR China

ARTICLE INFO

Article history:
Received 4 January 2008
Received in revised form 28 April 2008
Accepted 28 April 2008
Available online 4 May 2008

Keywords:
Solid oxide fuel cell
Plasma spraying
Coating
$La_{0.8}Sr_{0.2}Ga_{0.8}Mg_{0.2}O_3$ (LSGM)
Electrolyte

ABSTRACT

$La_{0.8}Sr_{0.2}Ga_{0.8}Mg_{0.2}O_3$ (LSGM) deposit in free standing planar shape was prepared by atmospheric plasma spraying (APS) to examine the coating microstructure and electrical conductivity to aim at applying APS LSGM to solid oxide fuel cells (SOFCs). The electrical conductivity of the plasma-sprayed LSGM coating was investigated. The coating microstructure was characterized by X-ray diffraction and scanning electron microscopy. The result showed that a fraction amorphous phase was present in the as-sprayed LSGM deposit, which starts to recrystallize at the temperature of 785 °C. The electrical conductivities of the LSGM with recrystallization treatment are 0.04 and 0.09 S cm^{-1} at 1000 °C at the directions perpendicular and parallel to the coating surfaces, respectively. The electrical conductivity at perpendicular direction is about one-tenth that of sintered bulk at 1000 °C. This result is due to the lamellar structure feature with the limited interface bonding which dominates the electrical conductivity of APS coatings. The activation energy for ion conduction within APS-deposited LSGM deposit depends on temperature range. The change of activation energy indicates that the ion transportation dominant changes with temperature.

1. Introduction

With the development of solid oxide fuel cell (SOFC), one of the major concerns is to reduce its operating temperature from 1273 K to that lower than 1073 K. A reduction of operating temperature will allow for easing the serious problems involved in high temperature operation, such as the materials selection of current collector and degradation of cell components. To reduce the operation temperature, utilizing the high ionic conductive materials than the conventional Y_2O_3 stabilized ZrO_2 (YSZ) as an electrolyte is much concerned recently. The perovskite oxide, $LaGaO_3$ doped with magnesium and strontium, exhibits a higher ionic conductivity than YSZ over a wide range of oxygen partial pressure with a typical conductivity about 0.10 S cm^{-1} at 800 °C [1,2]. It is therefore expected that the operating temperature of the SOFC can be decreased by using $LaGaO_3$-based oxide as the electrolyte of SOFC.

On the other hand, the commercialization efforts on SOFC systems are recently oriented to cost reduction in order to compete more effectively with other traditional power generating methods. Atmospheric plasma spraying (APS) is regarded as one of the most promising processing method for the production of solid oxide fuel cells because of its fast deposition rate and cost-effective characteristic compared with other film formation processes such as electrochemical vapor deposition (EVD) [1], vacuum plasma spraying (VPS) [2], sol–gel methods [3], dip-coating [4], sputtering [5], and so on. APS has been widely employed to fabricate anode [6], cathode [7], and interconnector [8] which are used to assemble SOFCs. Many attempts have been made to deposit electrolyte by APS. Although a fraction of porosity from several percent up to 20% can be formed in the thermal spray coatings [9], which may lead to significant gas permeation and limit the energy conversion efficiency, it was demonstrated that through post-spray densifying treatment the gas permeability of APS electrolyte can be adjusted to the level satisfactory for SOFC operation [10–13].

The previous investigations have shown that the dense APS YSZ coating can be obtained by impregnating yttrium and zirconium nitrate solution into the coating followed by heat treatment at 400 °C for 30 min [12,13], and the output performance of single cell fabricated by APS was promising. The open circuit voltage is comparable to the theoretical value and the maximum power density can reach 900 mW cm^{-2} [14]. Therefore, APS electrolyte with post-spray densifying treatment can also be applied to assemble SOFC.

In this study, the $La_{0.8}Sr_{0.2}Ga_{0.8}Mg_{0.2}O_3$ (LSGM) coating was deposited by APS and the coating microstructure and electrical conductivity were characterized. The influence of coating microstructure on its electrical conductivity was examined to

* Corresponding author. Tel.: +86 29 82665299; fax: +86 2982660970.
E-mail addresses: licx@mail.xjtu.edu.cn (C.-X. Li), xie.yingxin@zte.com.cn (Y.-X. Xie), licj@mail.xjtu.edu.cn (C.-J. Li), ygi@mail.xjtu.edu.cn (G.-J. Yang).

0378-7753/$ – see front matter © 2008 Elsevier B.V. All rights reserved.
doi:10.1016/j.jpowsour.2008.04.069

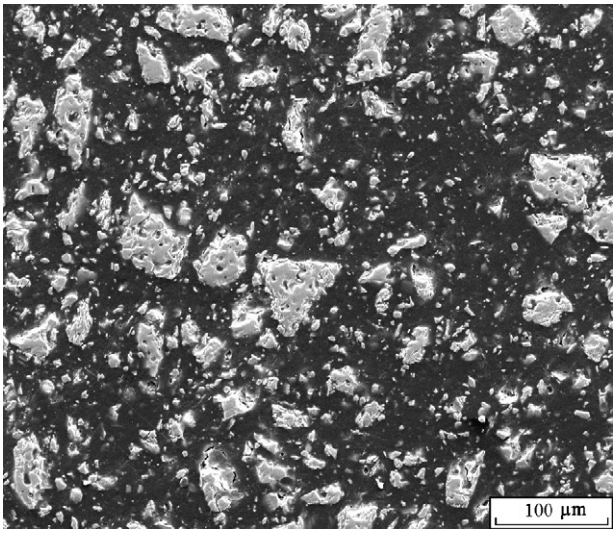

Fig. 1. Cross-sectional morphology of LSGM feedstock powders.

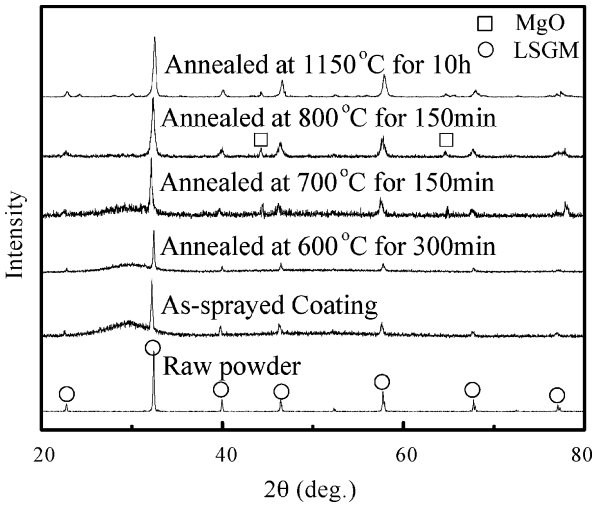

Fig. 2. XRD pattern of the as-sprayed LSGM coating in comparison with those of the starting powder and the annealed specimens.

reveal the dominant microstructure parameters over electrical conduction of APS LSGM coating.

2. Materials and experimental

2.1. Sample preparation

$La_{0.8}Sr_{0.2}Ga_{0.8}Mg_{0.2}O_3$ powder used for spray deposition in this study was prepared by a conventional solid phase reaction and sintering processes with La_2O_3, SrO, Ca_2O_3, and MgO. LSGM powders were embedded in epoxy resin for their microstructure examination. After metallographic grinding and polishing, the powder specimens were characterized using a scanning electron microscope. The cross-sectional morphology of LSGM feedstock is shown in Fig. 1. The nominal particle size ranges from 10 to 55 μm. The free standing LSGM specimens (Ø16 mm × 1.2 mm) was prepared by a commercial plasma spraying system (GDP-80, 80 kW class, JIUJIANG) under a plasma power of 22.4 kW (32 V × 700 A) and a spray distance of 100 mm. An Ar plasma was used to melt and accelerate the powders. Argon was used at 0.8 MPa. The flow of argon was fixed to 47 l min^{-1}. The LSGM coating was deposited with plasma jet traversing perpendicularly to sample surface. During spraying, the gun held horizontally was set to move over a support in a reciprocating manner at a speed of 320 mm s^{-1} with a step of 3 mm.

The crystalline structure of both powder and deposited coating was characterized by X-ray diffraction analysis (XRD) (Rigaku D/max-2400). Scanning electron microscope (SEM) was employed to characterize the morphology of powders and microstructure of the coating.

2.2. Measurement of electrical conductivity

The electrical conductivity of the LSGM deposit along the lamellar direction was measured by a four-probe dc method. The free standing specimens were 20 mm in length and 8 mm in width and approximately 700 μm in thickness. The measurement of electrical conductivity of LSGM coatings perpendicular to the lamellar direction was carried out using potentiostat/galvanostat based on a dc three-electrode approach from 600 to 1000 °C. The impedance spectroscopy was tested at a frequency range of 0.1 Hz to 30 kHz using a combined system of potentiostat/galvanostat and frequency response analyzer. Platinum slurry was pasted on both sides of the sample in an area of a diameter of 10 mm. The pasted sample was dried at 100 °C for 30 min and then heat-treated at 850 °C for 30 min. The heating rate was 5 °C min^{-1}. The platinum reference and counter electrodes were connected to one side of the sample, while the working electrode was connected to the other side. The electrical conductivity of the plasma-sprayed LSGM deposit, annealed at 850 °C for 30 min, at the directions perpendicular and parallel to the direction of LSGM deposit surface was measured.

3. Results and discussions

3.1. Microstructure of the plasma-sprayed LSGM

The XRD patterns of the as-sprayed LSGM coating and starting powder are shown in Fig. 2. From the XRD pattern, the starting LSGM feedstock only consisted of a single perovskite phase. However, a broad peak, which suggests the formation of an amorphous phase, was present in the XRD pattern of plasma-sprayed LSMG besides peaks of LSGM perovskite phase. The formation of the amorphous phase is associated with the rapid quenching of droplets in plasma spray process. This result was also reported by Ma et al. [15].

In order to determine the recrystallization temperature of the amorphous phase in the as-sprayed LSGM deposit, the DSC analysis was carried out at a heating and cooling rate of 5 °C min^{-1} at the ambient atmosphere. Fig. 3 shows the DSC curve obtained for the as-sprayed LSGM deposit. It can be seen from the DSC curve, an exothermic reaction took place at about 785 °C. It was considered that this reaction corresponds to the recrystallization of the amorphous phase in the as-sprayed deposit. To confirm the recrystallization of the as-sprayed LSGM deposit, the deposit was annealed at temperatures of 600, 700, and 800 °C and the XRD patterns of the annealed coatings were shown in Fig. 2. It can be found that full crystallization was achieved after a post-heat treatment at 800 °C for 150 min. This fact is consistent with the DSC analysis. It can also be found that the phase content did not change obviously when the deposits annealed at the temperature of 1150 °C for 10 h. However, from the XRD pattern, it is evident that a little amount of MgO phase was present in the post-annealed deposit.

Fig. 4a shows typical surface morphology of LSGM coating. It can be recognized that the coating was deposited by well-flattened particles. The vertical micro-cracks in flattened particles can be observed from the surface of the coating. This fact means that the LSGM coating was deposited by sufficiently molten spray parti-

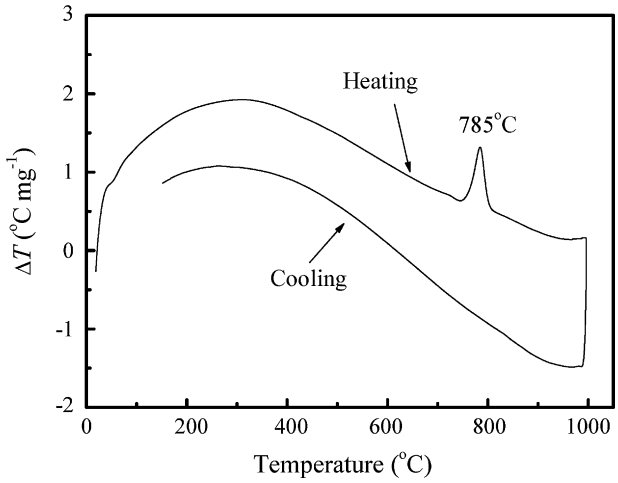

Fig. 3. DSC curve of the as-sprayed LSGM coating.

cles. Fig. 4b shows a typical morphology of fractured sample, by which the lamellar structure of plasma-sprayed ceramics is clearly revealed. It was clear that the coating consists of lamellar splats. The non-bonded interface between splats was evidently present in the coating. This is because a thermally sprayed deposit is formed by a stream of molten droplets impacting on the substrate followed by flattening, rapid solidification, and cooling processes and deposition of individual droplet is comparably independent. Fig. 4c shows a polished cross-sectional microstructure of APS LSGM coating obtained by SEM. The voids are present in the coating, resulting from the insufficient filling and incomplete wetting of molten liquid on previously formed rough coating surfaces. However, the lamellar structure is not clearly observed in Fig. 4c. This result is due to the limitation of the direct observation of the coating microstructure through microscopy analysis [16]. The lamellar structure feature of thermal spray coating with limited lamellar interface bonding leads to the anisotropy of coating properties and the reduction of electrical conductivity [12].

3.2. Electrical conductivity of the plasma-sprayed LSGM

Fig. 5 shows the electrical conductivity of the plasma-sprayed LSGM coating as a function of temperature. The electrical conductivity was measured at the both directions perpendicular and parallel to the coating surface. The electrical conductivity of LSGM coating in both directions increased with the increase of measurement temperature. The measurement yielded electrical conductivities of 0.04 and 0.09 S cm^{-1} at 1000 °C for the LSGM coating at the directions perpendicular and parallel to the coating surface, respectively. The electrical conductivity at parallel direction was about two times that along the perpendicular direction. This result clearly revealed that LSGM coating prepared by plasma spray presented an anisotropy in electrical conductivity.

According to the result reported by Ishihara et al. for LSGM with the same compositions as that used in the present study [17], the electrical conductivity of LSGM bulk will be about 0.4 S cm^{-1} at a temperature of 1000 °C. Therefore, it can be found that the electrical conductivity of LSGM coating along the direction perpendicular to coating surface is only about one-tenth that of LSGM bulk with the same compositions. On the other hand, the electrical conductivity at the direction parallel to coating surface was about one-fourth that of bulk material.

Thermally sprayed coating has a typical lamellar structure. Voids including the non-bonded interface between splats and vertical

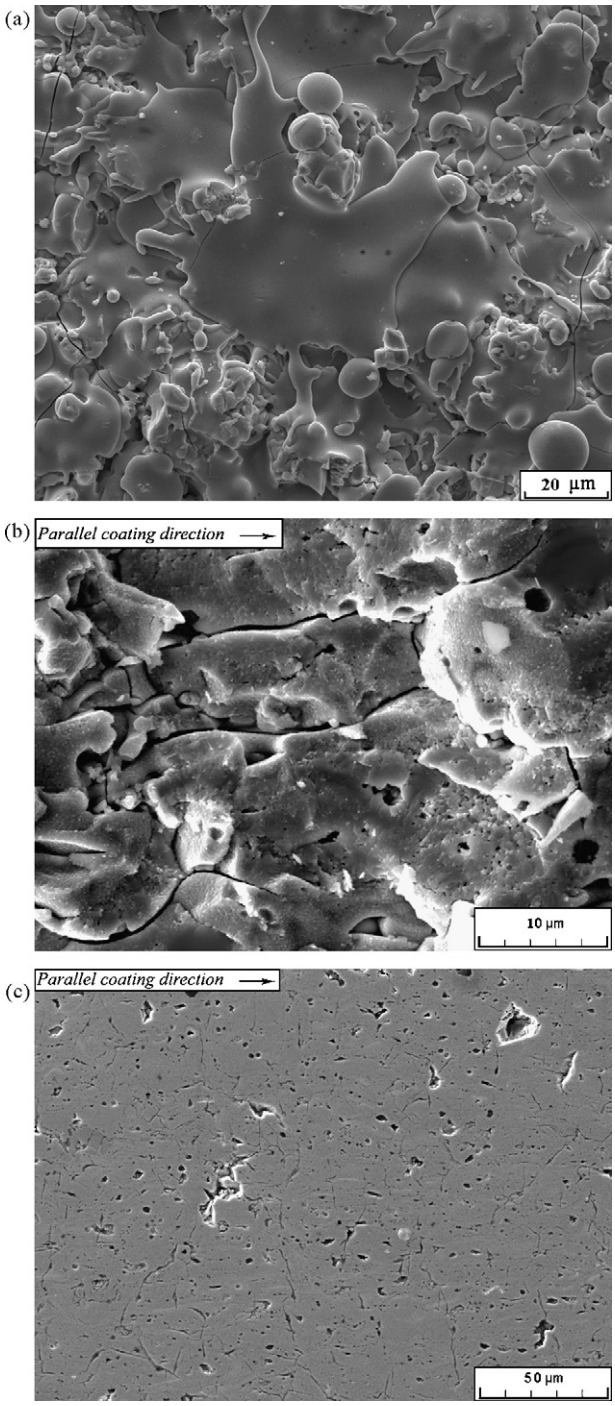

Fig. 4. Surface and cross-sectional morphology of plasma-sprayed LSGM coating: (a) surface morphology; (b) morphology of fractured cross-section; (c) mircostructure of polished cross-section.

cracks in individual splats are present in the coating. Only limited lamellar interfaces between splats in a plasma-sprayed ceramic deposit are bonded together. The maximum bonding ratio between lamellar interfaces, which is defined as the ratio of the total bonded interface area to the total apparent interface area, is about one-third total apparent interface [18]. The lamellar structure, especially fraction of the non-bonded interface area, dominates the mechanical and physical properties of the coating. The microstructural features of thermal spray coating leads obviously to not only reduction of coating parameters (e.g. mechanical properties including

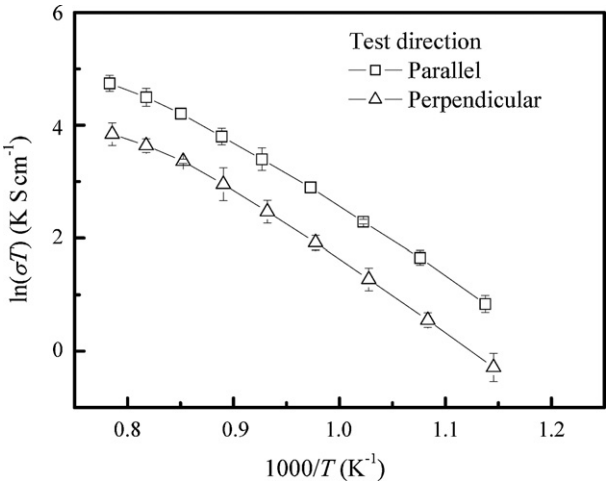

Fig. 5. Influence of temperature on the electrical conductivity of the plasma-sprayed LSGM measured at both the directions perpendicular and parallel to the coating surface.

Young's modulus, fracture toughness; thermal conductivity, electrical conductivity) but also the anisotropy in coating properties. The previous investigations have showed that the electrical conductivity of LSM [19] and YSZ [12] coating deposited by APS was one-fifth to one-third that of corresponding bulk materials. The electrical conductivity of plasma-sprayed LSGM coating obtained in this study is lower than those previous results.

It has been reported that the electrical conductivities of LSGM changes with different Sr and Mg concentrations. The conductivity of LSGM increases with the increase of Sr addition or Mg addition firstly, and after it reaches the maximum, then it tends to decrease [17,20–22]. The electrical conductivity of $La_{0.8}Sr_{0.2}Ga_{1-y}Mg_yO_3$ will be increased by 50% as the content of Mg increase from $y = 0.05$ to 0.2 [20]. It can be found from the XRD patterns as shown in Fig. 2 that a little amount of MgO phase was present in the post annealed deposit. Therefore, it was considered that the electrical conductivity of plasma-sprayed LSGM coating is dominated by two factors. One factor is the lamellar structure and bonding condition between lamellae in the coating and another one is the content of Mg which changed in the post-heat treatment.

3.3. Mechanism of electrical conduction of the plasma-sprayed LSGM coating

Fig. 6 shows the impedance spectra of the plasma-sprayed LSGM coating obtained at 950 °C in air. The resistance for ion transfer in a solid electrolyte consists of two parts: grain boundary resistance and intragrain resistance. The impedance spectroscopy can be employed to separate these contributions from the total resistance, which is interpreted with the aid of the parallel-connected resistor–capacitor (R–C) equivalent circuit [23]. With the equipment used in this study, two arcs were present in the spectra at high temperature test range. The intercept of left semicircle in the spectroscopy presents the grain boundary resistance of the coating (R_{gb}), while the intersection between the spectra at higher frequency and the real axial presents the intragrain resistance (R_g), and the low frequency semicircle is attributed to electrode response (R_{dl}) [23–25].

The temperature dependency of the intragrain and grain boundary conductivity of a typical plasma-sprayed LSGM coating determined by ac impedance technique was shown in Fig. 7. The total electrical conductivity was attributed to the sum of the intragrain and grain boundary resistances. It can be found that

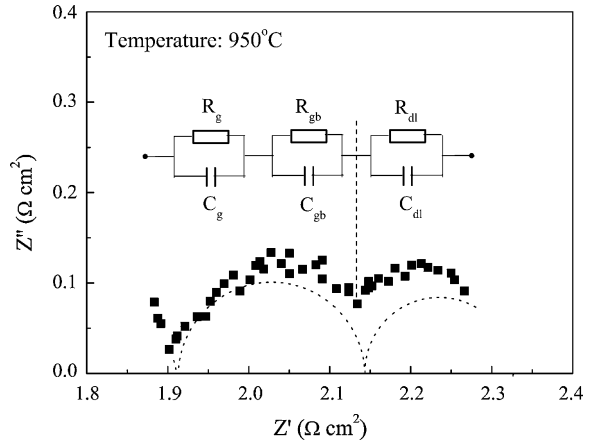

Fig. 6. Impedance spectra of the plasma-sprayed LSGM coating tested at 950 °C and the adopted R–C equivalent circuit.

the intragrain conductivity dominates the total conductivity at the temperature higher than 700 °C because the resistance of grain boundary is much less than the intragrain resistance, while with the decrease of temperature from 700 °C mentioned above the tendency in Fig. 7 shows that the influence of the grain boundary conductivity gradually becomes dominant over the total conductivity.

It is clear that the activation energy depends on temperature range. This phenomenon has been reported for zirconia- or ceria-based systems by several investigators [25–28] although the temperature where the activation energy changes is different with different systems. According to the intragrain–intergrain model [29], ion conduction will be dominated by the intragrain resistance in the high temperature regime and dominated by grain boundary resistance at lower temperatures. It can be found from Fig. 7 that the activation energy of grain boundary conductivity is higher than that of intragrain conductivity. The average activation energies of grain boundary and intragrain are 0.80 and 1.54 eV, respectively. It is reported that the presence of short-range order would increase the effective activation energy for ion conduction [20]. It is reasonable that the activation energy of grain boundary is higher than intragrain following the result reported by Huang et al. if grain boundary is regarded as short-range order region. Due to the difference of the activation energy of grain boundary from intragrain, the contribution of different regions to the total electrical conductivity *will*

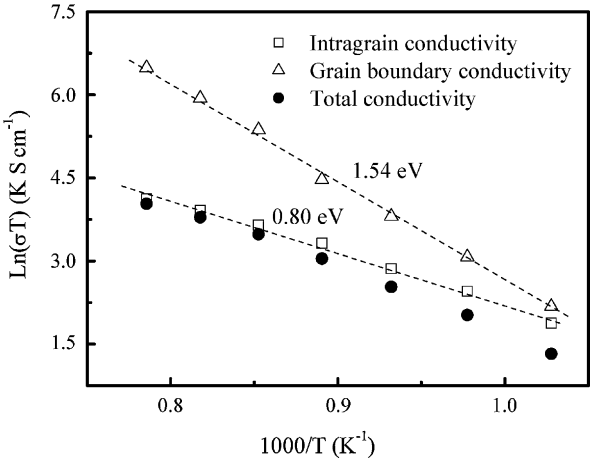

Fig. 7. Temperature dependency of the intragrain and grain boundary conductivities of plasma-sprayed LSGM determined by ac impedance technique.

changes with temperatures. This phenomenon is consistent with that observed for bulk LSGM [21]. Therefore, it is evident that the dominant factors to the ion conduction of LSGM deposit changes with temperature range.

4. Conclusions

The as-sprayed LSGM coating contained a fraction of amorphous phase resulting from the rapid quenching of droplets in plasma spray process. Full crystallization was achieved after a post heat treatment at a temperature of 800 °C. The plasma-sprayed coating presented a typically lamellar structure. The measurement yielded the electrical conductivities of 0.04 and 0.09 S cm^{-1} at 1000 °C for the LSGM coating at the directions perpendicular and parallel to the coating surface, respectively. The electrical conductivity at the perpendicular direction is about one-tenth that of sintered one at 1000 °C. This fact suggested that the lamellar structure feature with the limited interface bonding dominates the electrical conductivity of APS coating.

It was found that the activation energy for ion conduction within APS deposited LSGM deposit depends on temperature range. The results can be explained by the changing dominance of electrical conductivity from the grain boundary impedance at low temperature to the intragrain impedance at high temperature.

Acknowledgements

The present project was supported by National High Technology Research and Development Program of China (Granted no. 2007AA05Z135) and Research and Development of Science and Technology of Shaanxi Province (Granted no. 2006K07-G28).

References

[1] I. Minoru, M. Atsushi, Solid State Ionics 104 (1997) 303–310.
[2] M. Lang, R. Henne, S. Schaper, G. Schiller, J. Therm. Spray Technol. 10 (4) (2001) 618–625.
[3] S.G. Kim, S.P. Yoon, S.W. Nam, S.H. Hyun, S.A. Hong, J. Power Sources 110 (1) (2002) 222–228.
[4] Y.L. Zhang, J.F. Gao, D.K. Peng, G.Y. Meng, X.Q. Liu, Ceram. Int. 30 (2004) 1049–1053.
[5] A. Nagata, H. Okayama, Vacuum 66 (3/4) (2002) 523–529.
[6] H. Tsukuda, A. Notomi, N. Hisatome, J. Therm. Spray Technol. 9 (3) (2000) 364–368.
[7] K. Barthel, S. Rambert, S. Siegmann, J. Therm. Spray Technol. 9 (3) (2000) 343–347.
[8] L.J.H. Kuo, S.D. Vora, S.C. Singhal, J. Am. Ceram. Soc. 80 (3) (1997) 589–593.
[9] C.-J. Li, A. Ohmori, R. McPherson, J. Mater. Sci. 32 (1997) 997–1004.
[10] K. Okumura, Y. Aihara, S. Ito, S. Kawasaki, J. Therm. Spray Technol. 9 (2000) 354–359.
[11] K.A. Khor, L.G. Yu, S.H. Chan, X.J. Chen, J. Eur. Ceram. Soc. 23 (2003) 1855–1863.
[12] C.-J. Li, N.-X. Ning, C.-X. Li, Surf. Coat. Technol. 190 (1) (2005) 60–64.
[13] C.-J. Li, C.-X. Li, X.-J. Ning, Vacuum 73 (2004) 699–703.
[14] C.-J. Li, C.-X. Li, Y.-Z. Xing, M. Gao, G.-J. Yang, Solid State Ionics 177 (2006) 2065–2069.
[15] X.Q. Ma, H. Zhang, J. Dai, J. Roth, R. Hui, T.D. Xiao, D.E. Reisner, J. Therm. Spray Technol. 14 (2005) 61–66.
[16] C.-J. Li, W.-Z. Wang, Mater. Sci. Eng. A A386 (2004) 10–19.
[17] T. Ishihara, H. Matsuda, Y. Takita, J. Am. Ceram. Soc. 116 (1994) 3801–3803.
[18] A. Ohmori, C.-J. Li, Y. Arata, Trans. Jpn. Weld. Res. Inst. 19 (1990) 259–270.
[19] C.-J. Li, C.-X. Li, M. Wang, Surf. Coat. Technol. 198 (1–3) (2005) 278–282.
[20] K. Huang, M. Feng, J.B. Goudenough, J. Am. Ceram. Soc. 81 (2) (1998) 357–362.
[21] J.W. Stevenson, T.R. Armstrong, D.E. McCready, L.R. Pederson, W.J. Weber, J. Electrochem. Soc. 144 (10) (1997) 3613–3620.
[22] N. Liu, M. Shi, W. Wang, Y.P. Yuan, P. Majewski, F. Aldinger, J. Mater. Sci. 41 (13) (2006) 4205–4213.
[23] J. Ross Macdonald, Impedance Spectroscopy, Wiley, NY, 1987.
[24] J. Van Herle, A.J. McEvoy, K. Ravindranathan Thampi, J. Mater. Sci. 29 (1994) 3691–3701.
[25] I. Kosacki, H.U. Anderson, Y. Mizutani, K. Ukai, Solid State Ionics 152/153 (2002) 431–438.
[26] D.D. Edwards, J.-H. Hwang, S.J. Ford, T.O. Mason, Solid State Ionics 99 (1997) 85–93.
[27] D.Y. Wang, A.S. Nowick, J. Solid State Chem. 35 (1980) 325–333.
[28] A.I. Ioffe, M.V. Inozemtsev, A.S. Lipilin, M.V. Perfilev, S.V. Karpachov, Phys. Status Solidi A 30 (1975) 87–95.
[29] J.E. Bauerle, J. Hrizo, J. Phys. Chem. Solids 30 (1969) 565–570.